

A heavy load tire six-component force sensor

Zuoping Yao*, Yong Wei, Juncheng Lv

SAIC GM Wuling Automobile Co., Ltd., No.18 Hexi Road, Liunan District, Liuzhou, Guangxi Zhuang Autonomous Region, 545007, China

*Corresponding author: zuoping.yao@sgmw.com.cn

Abstract: This paper presents research on design and calibration of a heavy load tire six-component force (including three forces and three moments) sensor. Differ from common tire six-component force sensor, it is designed mainly for truck tire and aircraft tire test. With a four-column structure in its elastic body, size thinning in the middle of every column is designed to get a higher sensitivity in F_y channel. Before fabricating, the ‘virtual calibration’ is carried out, which proves that the design scheme of strain gauge position and elastic body matches well with each other. For there is low crosstalk between every two output channels. The calibration experiment results are not entirely the same as that in ‘virtual calibration’, for factors such as material heat treatment, machining accuracy and the quality of pasting strain gauges increase crosstalks. With decoupling calculation, a high-accuracy heavy load tire six-component force sensor is still obtained.

Keywords: heavy load, six-component force sensor, virtual calibration, decoupling calculation

1. Introduction

Tire six-component force sensor is widely used in the field of automotive development. For many crucial performances of automotive are closely related to tire mechanical properties. [1] Aircraft tire test usually done by ground test facilities and six-component force sensor (also called tire dynamometer) is a mainly used facility. [2] There are many tire test rigs such as MTS Flat Trac III and MTS Flat-Trac III CT plus in China. Their maximum vertical testing capacities are usually 25kN, so they are mainly used for the testing of passenger car tire and light truck tire. [3] In order to get the tire models to serve the development of heavy load truck and aircraft, a heavy load tire six-component force sensor is needed to obtain six-component force information of truck tire and tiny aircraft tire.

The heavy load tire six-component force sensor in this paper is of simple structure, which reduces the manufacturing difficulty and cost. Its measuring range is as follows:

$$F_x : -80kN \sim 80kN, \quad F_y : -60kN \sim 60kN, \quad F_z : 0kN \sim 80kN$$

$$M_x : -30kN m \sim 30kN m, \quad M_y : -30kN m \sim 30kN m$$

$$M_z : -30kN m \sim 30kN m.$$

Testing accuracy is one of the key technical character of tire six-component force sensor. During the process of design and fabricating, many factors cause a complicate coupling relationship, so it is difficult to decouple. [4] Low crosstalk between every two output channels is pursued by many scholars and manufacturers. [5-10] In fact, if the crosstalk coefficient is constant, it is possible to decouple and get a high-accuracy tire six-component force sensor. The heavy load tire six-component force sensor in this paper reduce the crosstalk by reasonable strain gauges position arrangement and measuring bridges at first. Then the decoupling calculation further ‘reduces’ the crosstalk on the premise of constant crosstalk coefficient.

This paper presents a heavy load tire six-component force sensor, which has heavy load in every force direction. It aims to solve the problem appeared in heavy load tire and tiny aircraft tire modeling tests.

The remainder of this paper is organized as follows. Section 2 introduces the structure of the tire six-component force sensor. Section 3 presents the ‘virtual calibration’ process by using Hypermesh and Abaqus softwares. The strain gauges position and measuring bridge is confirmed in this section. Section 4 describes the calibration experiment. The calibration experiment result is not entirely the same as that in ‘virtual calibration’. And there is a decoupling calculation. Section 5 is the conclusion of this paper.

2. Sensor Structure

The force sensor will be used on the tire test rig. As shown in Figure 1, one side of it should be connected to the test rig, and the other side should be connected to the rim of test tire.

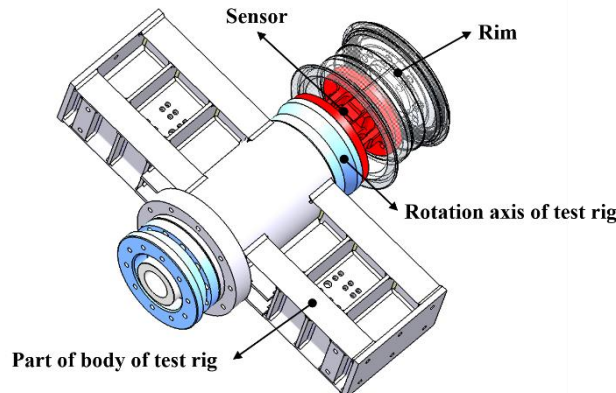


Figure 1: Installation position of the force sensor.

There are many types of structures for tire six-component force sensors. Kistler's tire six-component force sensor P530 is a typical product. As a kind of rigid quartz-based instrument, it has both fixed part and rotating part. Its sensing moments are fixed so rotating calculation is needless. The maximum vertical load of it is 30kN. Figure 2 is the outside drawing and assemble cross-section schematic of P530. [11]

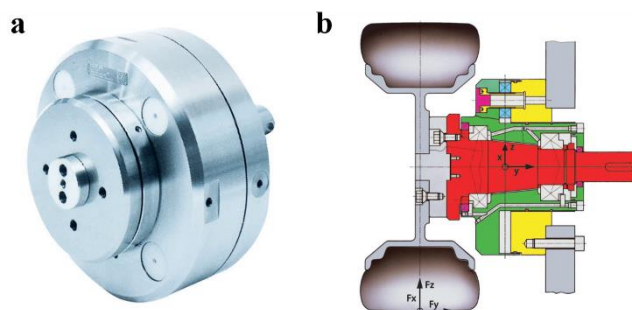


Figure 2: Kistler's tire six-component force sensor P530. (a) Outside drawing. (b) Assemble cross-section schematic.

Michigan Scientific Corporation has a series of tire six-component force sensors, and some of them have maximum vertical load more than 100kN. They usually have inner ring and outer ring. The sensor usually rotates with tire and special rim is needed, just as Figure 3 shows. [12]

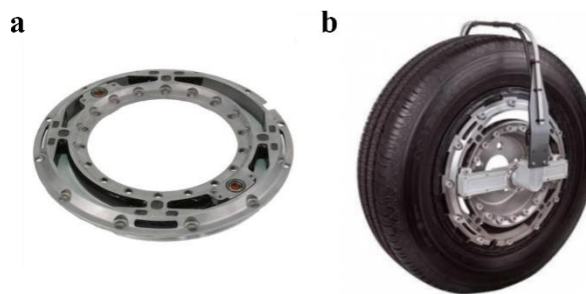


Figure 3: Tire six-component force sensor of Michigan Scientific Corporation. (a) Outside drawing. (b) Assemble schematic.

Considering the installation position and the structure of test rig. The force sensor in this paper is designed as an axial structure with four columns and it rotates with the rotation axis of test rig. Figure 4 shows the structure of this force sensor.

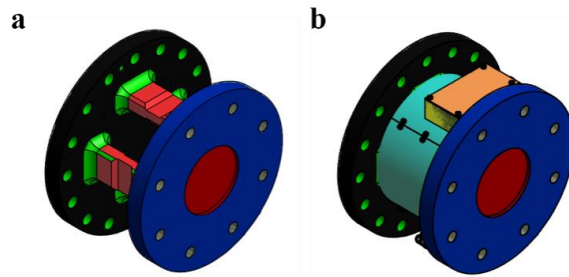


Figure 4: Heavy load tire six-component force sensor. (a) Model of the elastic body. (b) Model of the force sensor with shell.

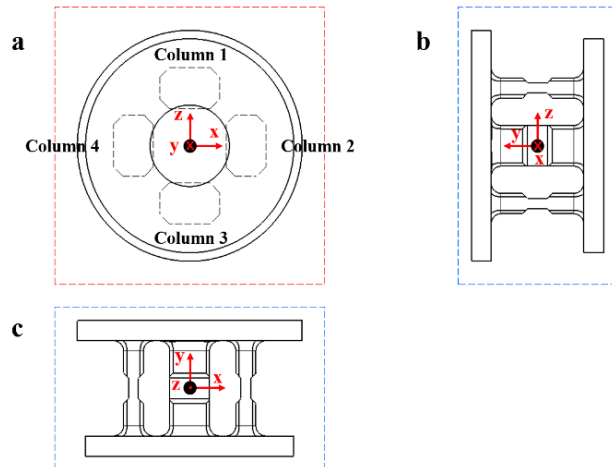


Figure 5: Shape three views of resistance strain tire six-component force sensor with four-column structure. (a) Front view (b) Left view (3) Top view

Figure 5 shows the diagrammatic of the force sensor. Strain gauges will be pasted on the planes of every column.

3. Virtual Calibration

Virtual calibration is in fact a kind of simulation technology. Simulation technology has been applied in many fields such as vehicle development, plane development and other machines' developments. [13-16] Virtual calibration is a convenient and effective method to determine the final size of elastic body and measurement scheme of strain gauges.

3.1 Meshing

The basic shape of elastic body is preliminary determined by the structure of test rig and the rim size of test tire. To taking the elastic into finite element analysis (FEA), preliminary treatment, which means meshing here is necessary. To guarantee the symmetry of elastic body as far as possible, one-eighth of the elastic body is meshed, as is shown in Figure 6.

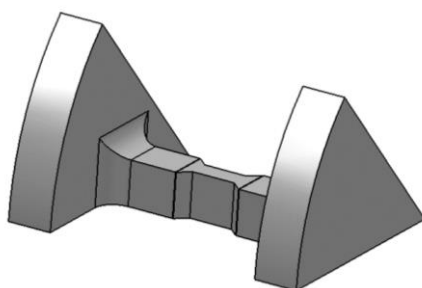


Figure 6: One-eighth of the elastic body to be meshed.

Parts where strain gauges will pasting on in the every column are divided into hexahedral elements

whose size is $1mm \times 1mm \times 1mm$. This is to facilitate the determination of strain gauges' positions. Other parts are divided into bigger size elements, for it is more efficient when simulating. The meshed one-eighth part turns into a whole model through reflecting and rotating commands. Figure 7 shows the whole meshed model and the mesh detail.

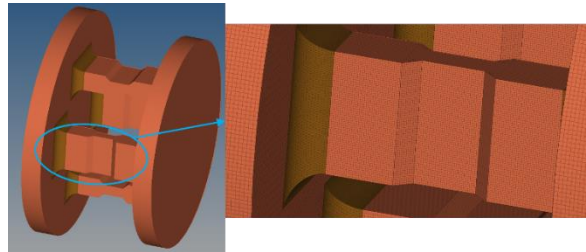


Figure 7: Meshed whole model and mesh detail.

3.2 Loading Simulation and Results

The loading simulation is carried out by Abaqus software. To get the ideal deformation, two flanges were set as rigid bodies. Flange on one side was fixed in six degrees and loads were transduced by flange on the other side. For the convenience of loading, a reference point was created at the origin of coordinate, which is coupled with the loads transducing flange. (See Figure 8.)

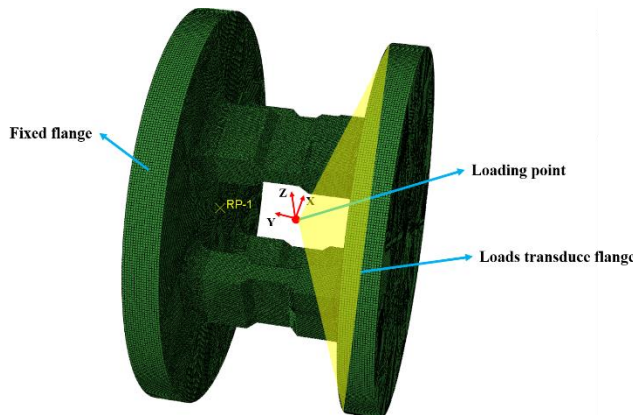


Figure 8: Loading simulation boundary conditions.

Loading F_x to M_z one by one, and according to the deformation and strain distribution under every load, the strain gauges' positions are determined. Figure 9 to 14 are the simulation results. Where in Figure 10, there are just strain gauges on one column. Strain gauges on other three columns are similar, so is the Figure 13. To show the deformations clearly, proper magnifications are used in visualization.

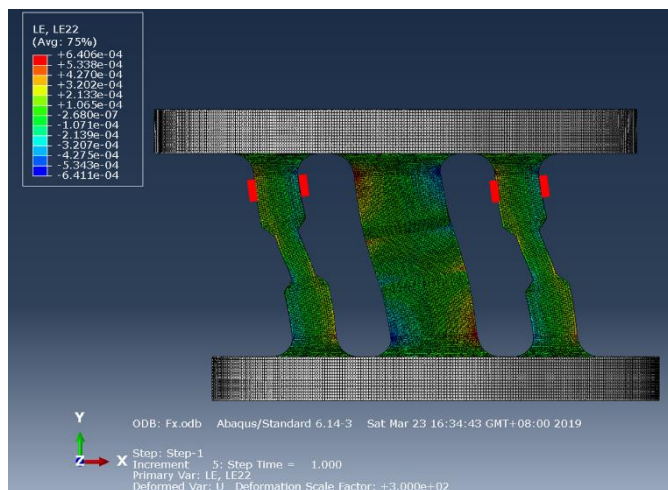


Figure 9: Simulation result under $F_x=80kN$ and strain gauges positions for F_x measurement channel.

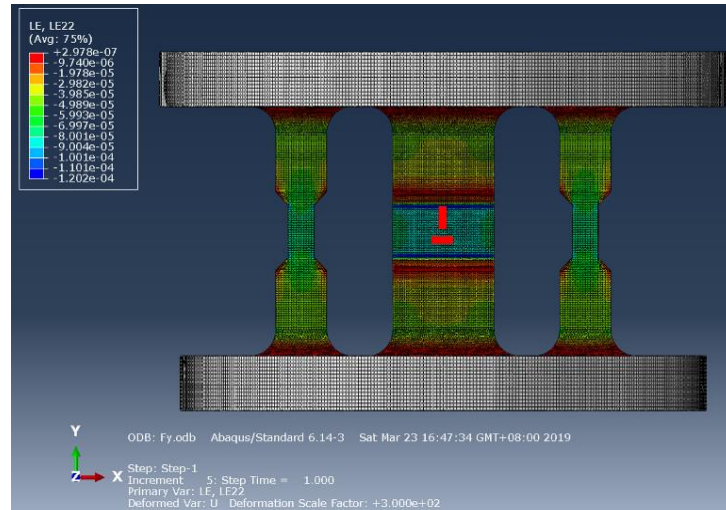


Figure 10: Simulation result under $F_y=60kN$ and strain gauges positions on one column for F_y measurement channel.

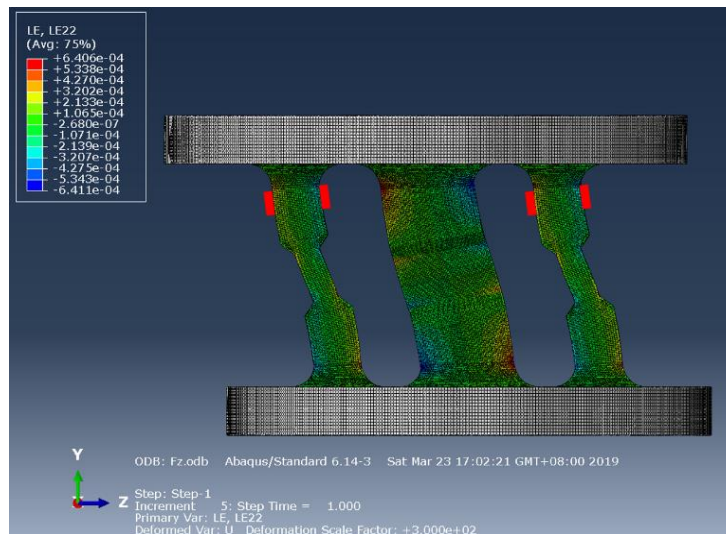


Figure 11: Simulation result under $F_z=80kN$ and strain gauges positions for F_z measurement channel.

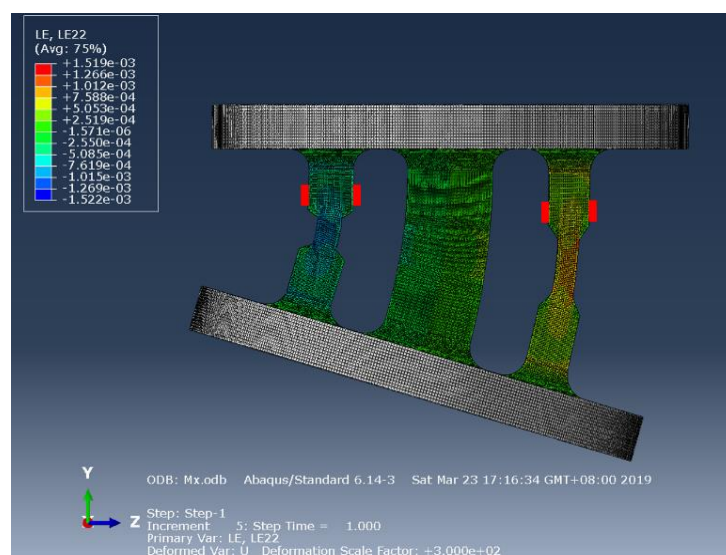


Figure 12: Simulation result under $M_x=30kN \cdot m$ and strain gauges positions for M_x measurement channel.

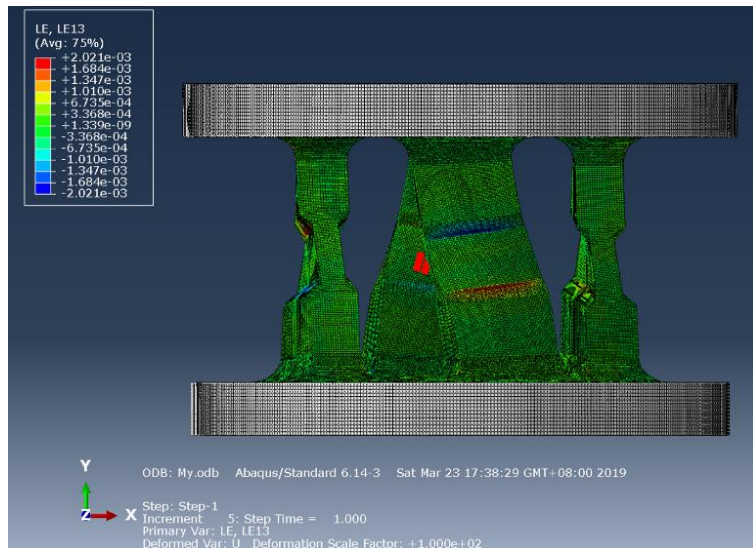


Figure 13: Simulation result under $M_y = 30\text{kN} \cdot \text{m}$ and strain gauges positions on one column for M_y measurement channel.

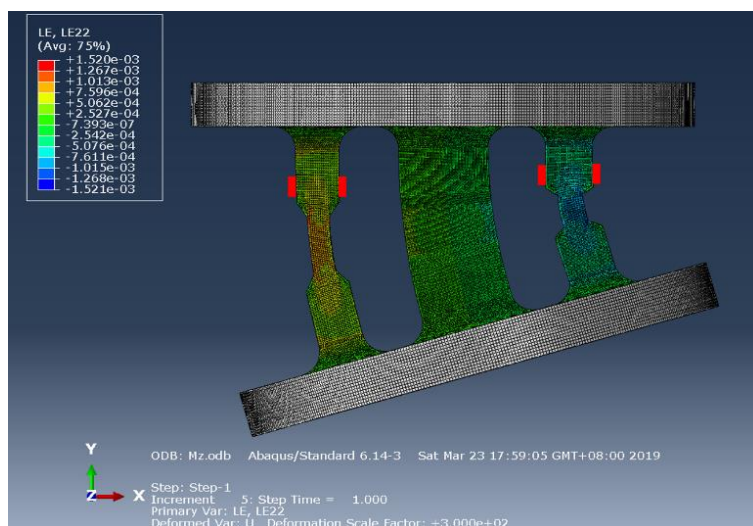


Figure 14: Simulation result under $M_z = 30\text{kN} \cdot \text{m}$ and strain gauges positions for M_z measurement channel.

The micro strain of output channel under every load is as shown in table 1. Table 1 shows that the sensitivity of F_y channel is lower than that of other channels. This is a defect of four-column elastic body. [17] A size thinning in the middle of every column is carried out to get a higher sensitivity, as is shown in Figure 5.

Table 1: Micro strain of output channel under every load

Load Channel Micro Strain	$F_x = 80\text{ kN}$	$F_y = 60\text{ kN}$	$F_z = 80\text{ kN}$	$M_x = 30\text{ kN} \cdot \text{m}$	$M_y = 30\text{ kN} \cdot \text{m}$	$M_z = 30\text{ kN} \cdot \text{m}$
F_x	928.333	0	0	0	0	9.167
F_y	0.390	-430.700	0.390	-0.167	0.221	-0.167
F_z	0	0	928.3	-9.167	0	0
M_x	0	0	0.167	1742.660	0	0
M_y	-0.012	-0.250	-0.012	-0.023	3998.945	-0.023
M_z	-0.167	0	0	0	0	1742.660

Table 2: Crosstalks between every two channels.

Load Output \ Load Output	F_x	F_y	F_z	M_x	M_y	M_z
F_x	/	0%	0%	0	0%	0.99%
F_y	-0.09%	/	-0.09%	0.04%	-0.05%	0.04%
F_z	0%	0%	/	-0.99%	0%	0%
M_x	0%	0%	0.01%	/	0%	0%
M_y	0%	0%	0%	0%	/	0%
M_z	-0.01%	0%	0%	0%	0%	/

As shown in table 2, crosstalks (FS) between every two channels can be got after ‘virtual calibration’. From table 2 the conclusions can be drawn:

- (1) F_y channel is affected by all other five channels.
- (2) There are crosstalks between F_x channel and M_z channels.
- (3) There are crosstalks between F_z channel and M_x channels.

Conclusion 1 can be explained by the low sensitivity of F_y channel. Conclusion 2 and 3 are caused by the measurement principle, they are inevitable under this strain gauges position scheme. But it is undeniable that results in table 2 represent a well-designed force sensor.

4. Calibration Experiment and Decoupling Calculation

To calibrate this heavy load tire six-component force sensor, a calibration device is fabricated. Figure 15 and 16 show its three-dimensional model.

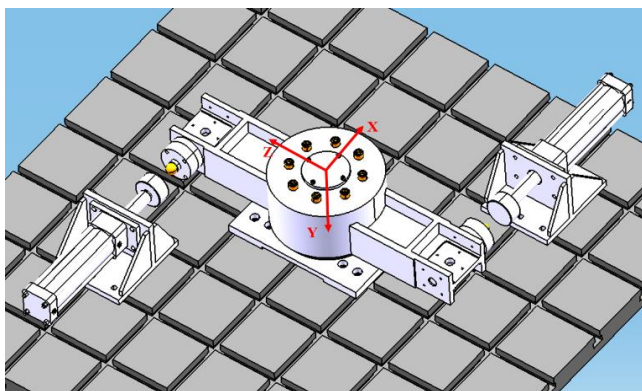


Figure 15: Calibration device model when loading M_y .

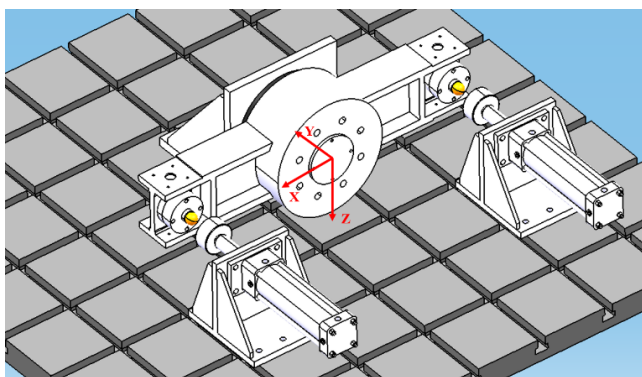


Figure 16: Calibration device model when loading F_y .

Considering the heavy load of this sensor, steel floor is used as the supporter. Two single-component force sensors whose accuracies are higher than 0.1% are used to measure loads. The load is applied by

two hydraulic cylinders. Figure 15 shows the model when loading M_y , and when the two hydraulic cylinders are put in the same side, F_x or F_z can be loaded. Figure 16 shows the model when loading F_y , and when the two hydraulic cylinders are put in the different side, M_x or M_z can be loaded.

Figure 17 shows the force sensor entity. It is taken into calibration experiment, as is shown in Figure 18.



Figure 17: Force sensor entity.



Figure 18: Calibration experiment.

The calibration experiment is carried out in loading and unloading process. For F_x and F_z channels, the loads are: 0kN-8kN-16kN-24kN-32kN-40kN-48kN-64kN-80kN-64kN-48kN-40kN-32kN-24kN-16kN-8kN-0kN. For F_y channel, the loads are: 0kN-6kN-12kN-18kN-24kN-30kN-36kN-48kN-60kN-48kN-36kN-30kN-24kN-18kN-12kN-6kN-0kN. For M_x , M_y and M_z channels, the loads are: 0kN m-3kN m-6kN m-9kN m-12kN m-15kN m-18kN m-24kN m-30kN m-24kN m-18kN m-15kN m-12kN m-9kN m-6kN m-3kN m-0kN m. Figure 19 to 24 show the calibration results under every load.

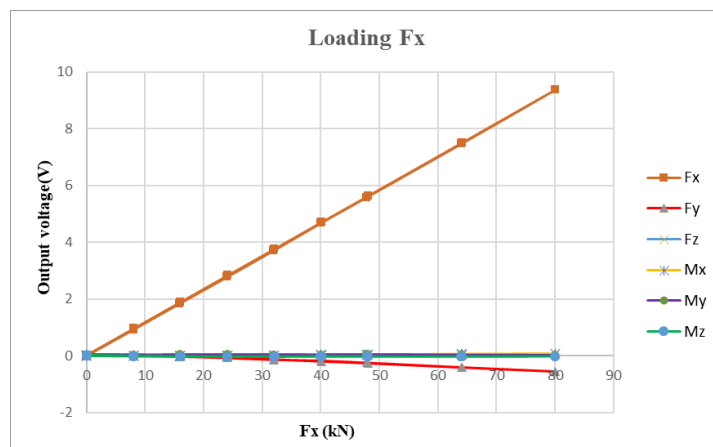
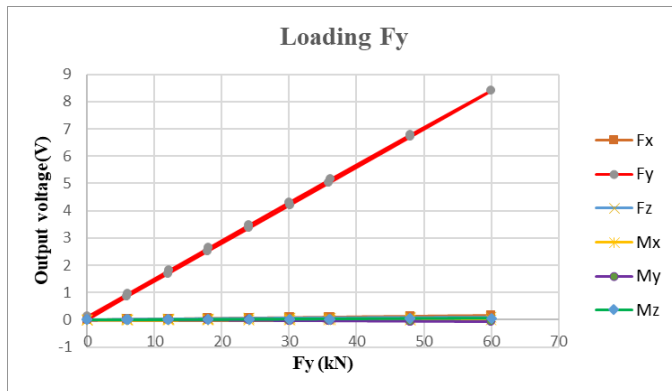
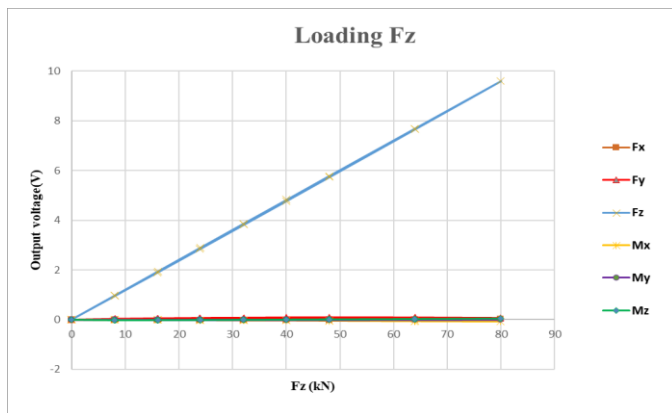
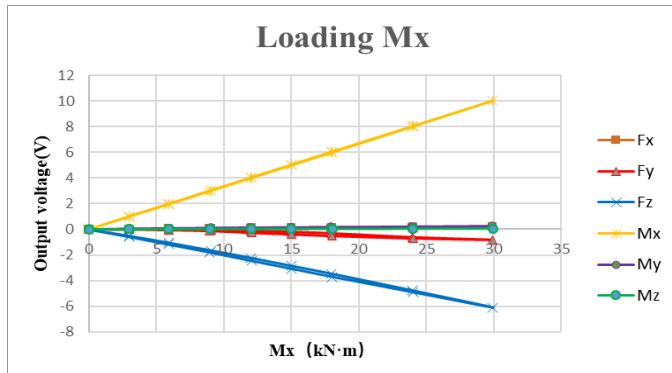
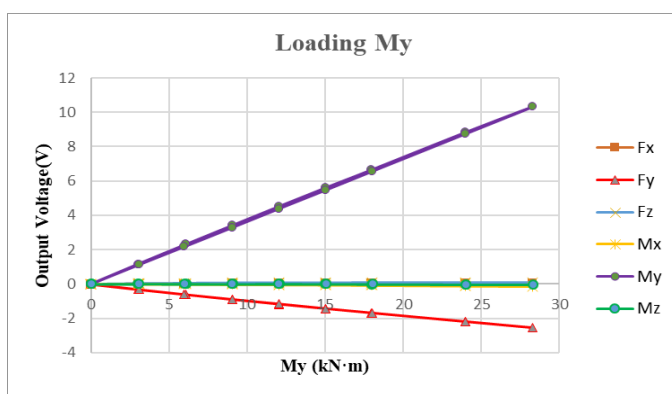


Figure 19: Calibration experiment result when loading F_x .

Figure 20: Calibration experiment result when loading F_y .Figure 21: Calibration experiment result when loading F_z .Figure 22: Calibration experiment result when loading M_x .Figure 23: Calibration experiment result when loading M_y .

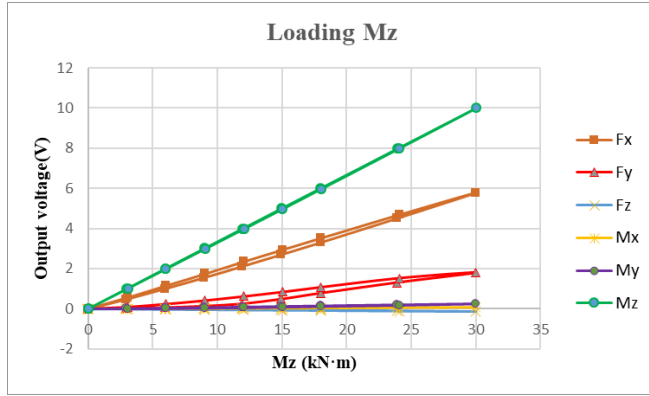
Figure 24: Calibration experiment result when loading M_z .

Figure 19 to 24 show there are several crosstalks that are obvious: F_x to F_y , M_x to F_y , M_x to F_z , M_y to F_y , M_z to F_x and M_z to F_y . This is caused by material heat treatment, machining accuracy, the quality of pasting strain gauges, signal acquisition and processing, etc. These crosstalk curves show that every crosstalk coefficient is almost unchanged, so decoupling calculation is available.

Calibration matrix is the relationship between load and six-component force sensor output voltage, which is shown in equation 1 and 2 [18-19].

$$\begin{bmatrix} U_1 \\ U_2 \\ U_3 \\ U_4 \\ U_5 \\ U_6 \end{bmatrix} = \begin{bmatrix} C_{11} & C_{21} & C_{31} & C_{41} & C_{51} & C_{61} \\ C_{12} & C_{22} & C_{32} & C_{42} & C_{52} & C_{62} \\ C_{13} & C_{23} & C_{33} & C_{43} & C_{53} & C_{63} \\ C_{14} & C_{24} & C_{34} & C_{44} & C_{54} & C_{64} \\ C_{15} & C_{25} & C_{35} & C_{45} & C_{55} & C_{65} \\ C_{16} & C_{26} & C_{36} & C_{46} & C_{56} & C_{66} \end{bmatrix} \cdot \begin{bmatrix} F_x \\ F_y \\ F_z \\ M_x \\ M_y \\ M_z \end{bmatrix} \quad (1)$$

$$\begin{bmatrix} F_x \\ F_y \\ F_z \\ M_x \\ M_y \\ M_z \end{bmatrix} = \begin{bmatrix} C_{11} & C_{21} & C_{31} & C_{41} & C_{51} & C_{61} \\ C_{12} & C_{22} & C_{32} & C_{42} & C_{52} & C_{62} \\ C_{13} & C_{23} & C_{33} & C_{43} & C_{53} & C_{63} \\ C_{14} & C_{24} & C_{34} & C_{44} & C_{54} & C_{64} \\ C_{15} & C_{25} & C_{35} & C_{45} & C_{55} & C_{65} \\ C_{16} & C_{26} & C_{36} & C_{46} & C_{56} & C_{66} \end{bmatrix}^{-1} \cdot \begin{bmatrix} U_1 \\ U_2 \\ U_3 \\ U_4 \\ U_5 \\ U_6 \end{bmatrix} \quad (2)$$

Where C_{ij} ($i=1,2\cdots 6, j=1,2\cdots 6$) is the coefficient of forces and moments worked on output voltage. i refers to the input load and j refers to the output voltage. For example, C_{23} is the coefficient that F_y works on U_3 . C^{-1} in equation 2 is the calibration matrix. After this calibration experiment, the C^{-1} can be got:

$$\begin{bmatrix} -8.53 & 0.21 & 0 & 0.13 & 0.06 & 4.97 \\ -0.42 & -7.19 & 0 & 0.03 & -1.94 & 0.24 \\ 0.01 & 0.09 & -8.38 & -5.01 & 0.12 & 0 \\ 0 & 0.01 & -0.02 & -3.00 & 0 & 0 \\ 0 & 0.03 & 0 & -0.04 & 2.80 & 0 \\ -0.01 & 0 & 0 & 0 & 0 & -3.00 \end{bmatrix}$$

Elements in C^{-1} are obtained by linear fitting. A non-crosstalk force sensor only has elements in the main diagonal of C^{-1} . Here in this paper, elements in other places of C^{-1} are added to reduce the influence of crosstalk.

5. Conclusions

In this study, the ‘virtual calibration’ and calibration experiment of the heavy load tire six-component force sensor are presented. The ‘virtual calibration’ shows a low crosstalk between every two channels.

The uncertain factors during fabrication and calibration experiment processes create higher crosstalks. Thanks to the subtle changes of crosstalk coefficients, decoupling calculation is available to get a high-accuracy force sensor.

There are still some inadequacies in this study. There was an accident during fabrication process, so the elastic body was not perfectly fabricated. The force sensor entity and calibration fixtures were not fixed tightly enough in calibration experiment, so the possible tiny displacement may cause a higher crosstalk. The tire test rig is still under upgrading, so the force sensor is not tested under rotation condition.

In future work, a new force sensor will be fabricated and calibrated in high quality. What's more, the rotation experiment will be carried out for the force sensor studied in this article and the new sensor.

Acknowledgements

This work was supported by Liuzhou Science and Technology Project [NO. 2018AA20501].

References

- [1] Guo, K.H., Liu, Y.B. and Yang, Y., *Development on tire test technology and prospect of its application in automobile performance research*. *Automobile Engineering*, (in Chinese), 1990(01): 3-11.
- [2] John F. Carter and Christopher J. Nagy, "The NASA Landing Gear Test Airplane," *NASA Dryden Flight Research Center; Edwards, CA, United States, June 01, 1995*, 96N18518
- [3] http://www.mts.com/cs/groups/public/documents/library/mts_006435.pdf
- [4] S. A. Liu, H. L. Tzo, "A Novel six-component force sensor of good measurement isotropy and sensitivities", *Sensors and Actuators A 100* (2002) 223-230
- [5] Hong, Daewoong, C. Li, and J. Jeong. "A Crosstalk Compensation of a Multi-axis Force Torque Sensor Based on the Least Squares Method Using LabVIEW." *Fourth International Conference on Computational & Information Sciences IEEE*, 2012. doi: 10.1109/ICCIS.2012.12
- [6] Zhang Jingzhu, "Study on Design Principle of Special Six-component Force Sensors," *Ph.D. thesis, College of Ordnance Science and Technology, Nanjing University of Science and Technology, Nanjing, 2008*
- [7] Feng, Lihang, et al. "Design and optimization of a self-decoupled six-axis wheel force transducer for a heavy truck." *Proceedings of the Institution of Mechanical Engineers, Part D: Journal of Automobile Engineering* 229.12 (2015): 1585-1610. doi: 10.1177/0954407014566439
- [8] Li, Ying Jun, et al. "A novel parallel piezoelectric six-axis heavy force/torque sensor." *Measurement* 42.5(2009):730-736. doi: 10.1016/j.measurement.2008.12.005
- [9] Pytka, J., "A Wheel Dynamometer for Off-Road Vehicles Testing," *SAE Technical Paper 2008-01-0783*, 2008, doi: 10.4271/2008-01-0783.
- [10] Wang Dong, "Research on Decoupling Theory and Technology of Automobile Wheel Force Measurement," *Ph.D. thesis, School of Instrument Science and Engineering, Southeast University, Nanjing, 2016*
- [11] <https://www.kistler.com/zh/product/type-9295b1/?application=14>
- [12] <http://www.msc-cn.com/products/transducers/wheel-force-transducers/>
- [13] Xiong, G.L., Li, B.H. and Chai, X.D, *Virtual Prototype Technology [J]. JOURNAL OF SYSTEM SIMULATION*, 2001, 13(1): 114-117.
- [14] Chen, P.F., Feng, J.Z., Liu, S.F., et al. *Research on the Performance of Car Suspension based on Computer Virtual Prototype Technology [J]. Computer and Modernization*, 2019(9).
- [15] Zhao, Y.Q., Bai, Y.Q., Ye C., et al. *Study on Static and Dynamic Characteristics of Mechanical Elastic Wheels [J]. China Mechanical Engineering*, 2019, 30(19): 2306-2312.
- [16] Lv, L., Wang, J.Z., Chen, S. *Control Stability Analysis of Electric Vehicle based on ADAMS [J]. Internal Combustion Engine & Parts*, 2019(14).
- [17] Gao Fei, "Numerical calculation and analysis of a six-component force transducer," *master's thesis, Transport College, Wuhan University of Technology, Wuhan, 2006*
- [18] Hai-Bin, L. I., et al. "New Calibration Method of Six-Axis Force Sensor Based on Stewart Platform." *Chinese Journal of Sensors and Actuators* 19.1(2006): 132-136. doi: 10.1016/S1005-8885(07)60041-7
- [19] Palli, G., et al. "Development of an optoelectronic 6-axis force/torque sensor for robotic applications." *Sensors and Actuators A: Physical* 220(2014): 333-346. doi: 10.1016/j.sna.2014.09.023